Electronic Supplementary Material (ESI) for Energy & Environmental Science.

Supplementary Information

Assessing Potential Profiles in Water Electrolysers to Minimise Titanium Use

Hans Becker[1], Edmund J.F. Dickinson[1], Xuekun Lu[1,2], Ulf Bexell[3], Sebastian Proch[3], Claire Moffatt[3], Mikael Stenström[3], Graham Smith[1], Gareth Hinds[1*]

[*]*Corresponding author: gareth.hinds@npl.co.uk*

[1]*National Physical Laboratory, Hampton Rd, Teddington, TW11 0LW, UK*

[2]*Electrochemical Innovation Lab, Department of Chemical Engineering, UCL, London, WC1E 7JE, UK*

[3]*Surface Research, Strategic Research, AB Sandvik Materials Technology, 81181 Sandviken, Sweden*

Contents:

Supplementary Note 1: Decoupling coefficient

If the deionised water in the PTL were somehow entirely electrically isolated from the CL, we would expect a certain OCP to be established in the PTL, independent of the CL potential and depending only on the PTL surface electrochemistry in the (oxygenated) deionised water environment. Conversely, if an infinitely conductive electrolyte connected the PTL to the CL, a uniform potential must apply throughout. We call these limits “decoupled” and “coupled” potential regimes, respectively. In the decoupled regime, the polarisation of the anode CL with respect to the cathode CL, which exists to apply sufficient overpotential to drive the OER at the desired rate, does not create a correspondingly polarising environment in the PTL local to the CC. This is because the high electrolyte resistance in the PTL region prevents anodic current density on the PTL material surface from being drawn through the PEM to the cathode CL.

We assume negligible electronic resistance through the solid parts of the PTL. Then, the extent of coupling between the CC-PTL OCP, measured by an *in situ* reference electrode, and the CL potential depends upon the relative magnitudes of the solution resistance through the PTL and the charge transfer resistance of the passive corrosion process on the PTL surface. This can be understood by considering the different conductive phases in the anode, as illustrated schematically in **Supplementary Figure 3**.

The potential difference between the anode CC and the reference electrode (RE), indicated by E_{loc}, will rest such that no net current flows in this circuit. Since a conductive path in the electrolyte phase links the CC to both the sites of the PTL corrosion reactions and the anode CL, E_{loc} will rest, in principle, between these two potentials such that it does not draw net current. The relative sensitivity of E_{loc} to the two processes depends on the electrolyte resistance between the RE tip and the sites of the two faradaic processes. When the RE tip is located at the CC-PTL interface, the electrolyte resistance will diminish the influence of the distant PEM such that E_{loc} is most strongly influenced by local corrosion processes in the PTL. In order for the RE measurement to approach the OCP of the PTL and so to be decoupled from the OER potential, we require the total PTL aqueous phase solution resistance $R_{\mathrm{soln,PTL}}$ to be high compared to the charge transfer resistance of the PTL passive corrosion processes, $R_{\mathrm{ct,PTL}}$. On this basis, we define a unitless potential decoupling coefficient Δ as follows:

$$\Delta = \frac{R_{\mathrm{soln,PTL}}}{R_{\mathrm{ct,PTL}}} \qquad \text{* MERGEFORMAT (1)}$$

When $\Delta ? 1$, the *in situ* RE measurement at the CC-PTL interface will be extensively decoupled from the anode CL and is expected to reflect the *ex situ* OCP in a medium of comparable ionic conductivity, pH and oxygenation.

We make the potential decoupling coefficient semi-quantitative using idealised expressions for the two lumped resistances in a homogeneous PTL. The solution resistance through the PTL thickness is expressed from an effective conductivity according to the standard formula for a prismatic resistor * MERGEFORMAT (2). To separate morphological and electrochemical properties of the PTL, effective electrolyte conductivity is expanded using porosity and tortuosity (3). The charge transfer resistance is defined from the exchange current density and interfacial surface area of the PTL material (4).[1]

$$R_{\mathrm{soln,PTL}} = \frac{L_{\mathrm{PTL}}}{A_{\mathrm{el}}} \frac{1}{\kappa_{\mathrm{eff,PTL}}} \qquad \text{* MERGEFORMAT (3)}$$

$$\kappa_{\mathrm{eff,PTL}} = \frac{\varepsilon_{\mathrm{PTL}}}{\tau_{l,\mathrm{PTL}} \rho_l} \qquad \text{* MERGEFORMAT (4)}$$

$$R_{\mathrm{ct,PTL}} = \frac{1}{A_{\mathrm{el}} L_{\mathrm{PTL}}} \frac{RT}{F} \frac{1}{i_{0,\mathrm{PTL}} a_{\mathrm{vol,PTL}}} \qquad \text{* MERGEFORMAT (5)}$$

Thus:

$$\Delta = \rho_l \left(L_{\mathrm{PTL}}^2 \frac{a_{\mathrm{vol,PTL}} \tau_{l,\mathrm{PTL}}}{\varepsilon_{\mathrm{PTL}}} \right) \left(\frac{RT}{F i_{0,\mathrm{PTL}}} \right)^{-1} \qquad \text{* MERGEFORMAT (6)}$$

The potential decoupling coefficient is expressed in * MERGEFORMAT (6) as the product of three terms:

1. The resistivity ρ_{l} of the water used in the PEMWE.
2. The geometric and morphological properties of the PTL (total thickness, tortuosity, porosity, interfacial surface area).
3. The kinetic properties of the PTL passive corrosion process.

Clearly, greater decoupling of the CC from the anode CL is expected with more resistive deionised water, and with a thicker or more tortuous PTL. It should be noted here that, while more rapid kinetics of the passive corrosion process at the PTL corresponds to an increased degree of decoupling, a lower anodic polarisation is required to achieve a given anodic current density as the kinetics become faster. Hence, greater potential decoupling is no guarantee of greater corrosion resistance, when comparing different chemical systems.

The data collated for the experimental system allow evaluation of the potential decoupling coefficient. Using the data collated in Supplementary Table 1, and considering only the sinter portion of the PTL, the potential decoupling coefficient evaluates to $\Delta \approx 2500$. Thus the anode CC-PTL potential is predicted from simple theory to be significantly decoupled under standard

operating conditions; this prediction is consistent with the previous *in situ* measurement of a decoupled E_{loc} for an RE located at the anode CC.[2]

Supplementary Note 2: Physicochemical model formulation

The simple model used to derive the potential decoupling coefficient reveals the most important factors governing the *in situ* potential experienced at the CC-PTL interface. It does not give detail, however, concerning the potential profile through the PTL thickness. A 1D physical model is now formulated to address these questions in greater detail, resolving the anode side of the cell in the current flow direction subject to the following approximations:

- The PEMWE is considered to be homogeneous in the plane of the electrodes.
- The cathode is assumed to behave ideally (zero overpotential).
- The cell is assumed to be isothermal (uniform temperature).
- All porous media are treated as locally homogenised, with their morphology expressed by a local porosity and tortuosity.
- Mass transfer effects are neglected.

The anode side of the cell is divided into four regions: Mesh, Sinter, CL, and Membrane. The potential distribution is assessed by means of the following current distribution model, resolved along the electrode-normal coordinate x. Notation is summarised in Supplementary Table 2 and parameterisation of inputs is given in Supplementary Table 3. The anode mesh–piston interface is at $x = 0$ and the membrane-cathode interface is at $x = L_{\mathrm{tot}}$.

Electrode current conservation:

$$\frac{di_{s,\mathrm{eff}}}{dx} = -i_{\mathrm{vol},m} \quad (m = \text{Mesh, Sinter, CL}) \text{ * MERGEFORMAT (7)}$$

$$i_{s,\mathrm{eff}} = -\sigma_{\mathrm{eff},m}\frac{d\phi_s}{dx} \quad (m = \text{Mesh, Sinter, CL}) \text{ * MERGEFORMAT (8)}$$

Electrolyte current conservation:

$$\frac{di_{l,\mathrm{eff}}}{dx} = i_{\mathrm{vol},m} \quad (\text{all regions } m) \text{ * MERGEFORMAT (9)}$$

$$i_{l,\mathrm{eff}} = -\kappa_{\mathrm{mem}}\frac{d\phi_l}{dx} \quad (\text{Membrane}) \text{ * MERGEFORMAT (10)}$$

$$i_{l,\mathrm{eff}} = -\kappa_{\mathrm{mem}}\frac{\varepsilon_{\mathrm{CL}}}{\tau_{\mathrm{CL}}}\frac{d\phi_l}{dx} \quad (\text{CL}) \text{ * MERGEFORMAT (11)}$$

$$i_{l,\mathrm{eff}} = -\kappa_{\mathrm{w}}\frac{\varepsilon_k}{\tau_k}\frac{d\phi_l}{dx} \quad (k = \text{Mesh, Sinter}) \text{ * MERGEFORMAT (12)}$$

Effective volumetric current density:

$$i_{\mathrm{vol,mem}} = 0 \qquad \text{* MERGEFORMAT (13)}$$

$$A_{\mathrm{a,OER}} \log_{10}\left(\frac{i_{\mathrm{vol,CL}} L_{\mathrm{CL}}}{i_{\mathrm{ref,sp,OER}} m_{\mathrm{ano}}}\right) = \phi_s - \phi_l - E_{\mathrm{ref,OER}} \qquad \text{* MERGEFORMAT (14)}$$

$$i_{\mathrm{vol},k} = i_{0,\mathrm{PTL}} a_{\mathrm{vol},m} \frac{F}{RT}\left(\phi_s - \phi_l - E_{\mathrm{corr,PTL}}\right) \quad (k = \text{Mesh, Sinter}) \text{ * MERGEFORMAT (15)}$$

Electric ground is defined at the mesh-piston interface:

$$\phi_{s,x=0} = 0 \qquad \text{* MERGEFORMAT (16)}$$

A defined cell current density is applied at the membrane-cathode interface:

$$i_{l,x=L_{\mathrm{tot}}} = i_{\mathrm{cell}} \qquad \text{* MERGEFORMAT (17)}$$

The cell voltage is evaluated as:

$$E_{\mathrm{cell}} = -\phi_{l,x=L_{\mathrm{tot}}} \qquad \text{* MERGEFORMAT (18)}$$

The local *in situ* potential measured between the anode CC and the reference electrode is given as:

$$\begin{aligned} E_{\mathrm{loc}} &= \phi_{s,x=0} - \phi_l \\ &= -\phi_l \end{aligned} \qquad \text{* MERGEFORMAT (19)}$$

All equations were solved in COMSOL Multiphysics 5.6 (COMSOL AB, Stockholm, Sweden) using the **Secondary Current Distribution** physics interface with user-defined modifications as required to express the mathematically specified equations. Computations were performed on standard desktop computing hardware. The 1D geometry was resolved with 100 elements in the CL, maximum global mesh element size 33.1 µm, and maximum mesh element growth rate 1.05 (PTL) and 1.1 (membrane).

The product of two key parameters, $i_{0,\mathrm{PTL}}$ and PTL volumetric surface area ($a_{\mathrm{vol,PTL}}$), significantly influences the degree of potential decoupling. For a quoted activation energy of ≈ +105 kJ mol^{-1},[3] $i_{0,\mathrm{PTL}}$ increases by about 2 orders of magnitude at 60 °C compared to 25 °C. The precise value of $a_{\mathrm{vol,PTL}}$ may also be difficult to obtain experimentally due to associated uncertainty. The model uncertainty is therefore defined as 1 order of magnitude around the assumed value of the product $i_{0,\mathrm{PTL}} \times a_{\mathrm{vol,PTL}}$. Higher values of these quantities will increase the potential decoupling, but will also lower the required degree of polarisation for appreciable anodic corrosion of the PTL. Corresponding experimental comparisons are shown in the main text (Figure 1b) as well as **Supplementary Figure 1** and **Supplementary Figure 2**. **Supplementary Figure 10** shows that the extent of polarisation to over 100 mV above OCP ranges from 0.1 to 1 mm away from the anode CL in Type II deionised water, depending on the precise parameterisation.

Supplementary Note 3: Water and dilute H_2SO_4(aq) conductivity at 60 °C

The conductivity of Type I water at 60 °C was obtained as referenced in ASTM D 1125 - 95 (2005).[4] For Type II water and dilute H_2SO_4(aq), variation of conductivity κ as a function of temperature was estimated based on a Stokes-Einstein-like dependence on temperature T and dynamic viscosity μ, leading to an estimated increase in κ by a factor of 2 on transition from room temperature to 60 °C.

$$\frac{\kappa}{\kappa_{\mathrm{ref}}} = \frac{T}{T_{\mathrm{ref}}} \frac{\mu_{\mathrm{ref}}}{\mu} \qquad \text{* MERGEFORMAT (20)}$$

Supplementary Note 4: *Ex situ* determination of interfacial contact resistance change for bare 316L and C-316L @ 0.9 V vs RHE

Due to the contamination of the anode end flow plates that was observed following the single cell PEMWE tests a *post mortem* determination of the interfacial contact resistance (ICR) was not possible. Therefore, an *ex situ* electrochemical experiment was carried out replicating the *in situ* conditions: 0.9 V vs RHE, 60 °C, pH 4.5 (H_2SO_4), oxygen-saturated, 7 days. The results of these measurements are shown in Supplementary Figure 11 and the inset presents the current density at the beginning of the experiment. The higher current density observed for bare 316L (orange trace) in the inset is attributed to migrational oxide film growth. Supplementary Table 6 presents the results of the *ex situ* ICR measurements obtained by sandwiching the samples between two carbon fibre gas diffusion layers (GDLs) at a clamping pressure of 1.4 MPa. It is apparent that the ICR of C-316L is two orders of magnitude lower than for the uncoated alloy. Moreover, the contact resistance of the carbon-coated material does not change after the electrochemical experiment within the margins of error. It is, furthermore, suggested that the substantial ICR change for 316L is due to oxide film growth as reflected in the higher currents at the beginning of the electrochemical experiment.

Supplementary Table 1: Variables used in definition and assessment of lumped potential decoupling coefficient. Values indicated are for the experimental condition studied; "n/a" indicates variables that are not inputs for the eventual assessment of the coefficient value.

Symbol	Unit	Description	Value
A_{el}	m^2	Electrode area	n/a
$a_{\mathrm{vol,PTL}}$	m^{-1}	Surface area (electrode-electrolyte interface) of PTL per unit volume	2×10^4 m^{-1}
F	C mol^{-1}	Faraday constant	96485 C mol^{-1}
$i_{0,\mathrm{PTL}}$	A m^{-2}	Effective exchange current density, passive corrosion process at PTL	2×10^{-4} A m^{-2}
L_{PTL}	m	Thickness, PTL	2.1 mm
R	J K^{-1} mol^{-1}	Gas constant	8.3145 J K^{-1} mol^{-1}
$R_{\mathrm{ct,PTL}}$	Ω	Charge transfer resistance, passive corrosion process at PTL	n/a
$R_{\mathrm{soln,PTL}}$	Ω	Electrolyte solution resistance across PTL	n/a
T	K	Temperature	60 °C
Δ	1	Potential decoupling coefficient	evaluated
$\varepsilon_{\mathrm{PTL}}$	1	Porosity, PTL	0.15
$\kappa_{\mathrm{eff,PTL}}$	S m^{-1}	Effective conductivity, electrolyte in PTL	n/a
ρ_l	Ω·m	Bulk resistivity, electrolyte in PTL	10^5 Ω·m
τ_{PTL}	1	Tortuosity, PTL	6.47

Supplementary Table 2: Spatially resolved variables in 1D PEMWE anode potential distribution simulation.

Variable	Unit	Definition
E_{loc}	V	Voltage measured between working electrode (piston) and *in situ* RE at a location in the electrolyte
$i_{l,\mathrm{eff}}$	A m^{-2}	Effective electrolyte current density
$i_{\mathrm{s,eff}}$	A m^{-2}	Effective electrode current density
$i_{\mathrm{vol},m}$	A m^{-3}	Volumetric current density in porous region *m*
x	m	Spatial coordinate (electrode-normal)
ϕ_l	V	Electrolyte potential
ϕ_s	V	Electronic potential, electrode phase

Supplementary Table 3: Symbols and values (5 s.f.) of specified input parameters to 1D PEMWE anode potential distribution simulation.

Symbol	Value	Definition	Source
$a_{\mathrm{vol,mesh}}$	3×10^3 m^{-1}	Volumetric surface area, anode mesh	Estimated from X-ray CT measurement
$a_{\mathrm{vol,sinter}}$	2×10^4 m^{-1}	Volumetric surface area, anode PTL	Electrochemical active surface area measurement
$A_{\mathrm{a,OER}}$	58 mV	Anodic Tafel slope, oxygen evolution reaction	Fit to polarisation curve
$E_{\mathrm{corr,PTL}}$	1 V vs RHE	OCP (or corrosion potential), anode mesh/PTL	*Ex situ* measurement
$E_{\mathrm{ref,OER}}$	1 V vs RHE	Reference Tafel slope potential, oxygen evolution reaction	Defined
F	96485 C mol^{-1}	Faraday constant	Defined by SI
i_{cell}	up to 3 A cm^{-2}	Cell operating current density	Experimental specification
$i_{\mathrm{ref,vol,OER}}$	2×10^{-4} mA g^{-1}	Specific reference current density, oxygen evolution reaction	Fit to polarisation curve
$i_{0,\mathrm{PTL}}$	2×10^{-4} A m^{-2}	Exchange current density, passive corrosion process, anode mesh/PTL	Calculated from reference[3]
L_{CL}	30 µm	Thickness, anode CL	*Ex situ* SEM of MEA
L_{mem}	127 µm	Thickness, membrane	Conventional dry thickness of Nafion 115
L_{mesh}	1 mm	Thickness, anode mesh	Experimental configuration (measured)
L_{sinter}	2.1 mm	Thickness, anode PTL	Experimental configuration (measured)
L_{tot}	3.308 mm	Total anode side and membrane thickness	Experimental configuration
m_{ano}	3 mg cm^{-2}	Mass loading of catalyst, anode	Manufacturer's specification
R	8.3145 J K^{-1} mol^{-1}	Gas constant	Defined by SI
T	60 °C	Temperature	Experimental configuration
$\varepsilon_{\mathrm{CL}}$	0.5	Porosity, anode CL	Assumed
$\varepsilon_{\mathrm{mesh}}$	0.51	Porosity, anode mesh	X-ray CT measurement
$\varepsilon_{\mathrm{sinter}}$	0.15	Porosity, anode PTL	X-ray CT measurement
κ_{mem}	9.5 S m^{-1}	Electrolyte conductivity, membrane	Fit to polarisation curve, compatible with literature
κ_{w}	0.25 µS cm^{-1} 2 µS cm^{-1} 80 µS cm^{-1} 800 µS cm^{-1}	Electrolyte conductivity, water ASTM Type I water ASTM Type II water pH 4 H_2SO_4 (aq)	See Supplementary Note 3

	8×10^{-4} µS cm^{-1}	pH 3 H_2SO_4 (aq) pH 1 H_2SO_4 (aq)	
$\sigma_{eff,CL}$	100 S m^{-1}	Effective electrode conductivity, anode CL	Assumed, set infinite in main text Figure 2a
$\sigma_{eff,mesh}$	1000 S m^{-1}	Effective electrode conductivity, anode mesh	Assumed, set infinite in main text Figure 2a
$\sigma_{eff,sinter}$	1000 S m^{-1}	Effective electrode conductivity, anode PTL	Assumed, set infinite in main text Figure 2a
τ_{CL}	2	Tortuosity, anode CL	Assumed
τ_{mesh}	1.5	Tortuosity, anode mesh	X-ray CT measurement
τ_{sinter}	6.47	Tortuosity, anode PTL	X-ray CT measurement

Supplementary Table 4: Comparison of ICR of C-304L before and after potential hold in oxygen-saturated H_2SO_4 (pH 3), 0.1 ppm HF, at 70 °C for 18 h.

C-304L	ICR* (as-received)	ICR* (after 18 h)
1.0 V vs RHE	2.5 ± 0.2 mΩ cm^2	2.5 ± 0.2 mΩ cm^2
1.2 V vs RHE	2.5 ± 0.2 mΩ cm^2	5.3 ± 0.2 mΩ cm^2
1.4 V vs RHE	2.5 ± 0.2 mΩ cm^2	5.2 ± 0.2 mΩ cm^2
1.6 V vs RHE	2.5 ± 0.2 mΩ cm^2	200 mΩ cm^2

* interfacial contact resistance vs. carbon-fibre GDL (1.4 MPa)

Supplementary Table 5: Concentration of selected impurities inside the CCM and in the anode/cathode feed water before and after testing.

	Ti / ppm	Cr / ppm	Mn / ppm	Fe / ppm	Mo / ppm
CCM Batch 1 (as-received)	< 0.5	0.6 ± 0.1	0.25 ± 0.05	< 2	< 0.1
CCM Batch 1 (2 A cm^{-2}, 316L, 7 days)	< 0.5	0.8 ± 0.1	0.4 ± 0.1	< 2	< 0.1
CCM Batch 1 (2 A cm^{-2}, C-316L, 7 days)	1.4 ± 0.2	0.7 ± 0.1	0.4 ± 0.1	< 2	< 0.1
CCM Batch 2 (as-received)	< 0.5	0.39 ± 0.06	0.24 ± 0.05	1.4 ± 0.2	< 0.05
CCM Batch 2 (2 A cm^{-2}, C-316L, 30 days)	< 0.5	< 0.1	< 0.1	< 1	< 0.05
Anode water tank* (before 30 day test, C-316L)	1.2 x 10^{-3}	0.4 x 10^{-3}	0.1 x 10^{-3}	2.5 x 10^{-3}	3.5 x 10^{-4}
Anode water tank* (after 30 day test, C-316L)	1.2 x 10^{-3}	0.3 x 10^{-3}	1.1 x 10^{-4}	2.7 x 10^{-3}	0.3 x 10^{-3}
Cathode water tank* (before 30 day test, C-316L)	1.6 x 10^{-3}	0.3 x 10^{-3}	0.09 x 10^{-3}	2.1 x 10^{-3}	1.7 x 10^{-3}
Cathode water tank* (after 30 day test, C-316L)	2.1 x 10^{-3}	0.3 x 10^{-3}	0.19 x 10^{-3}	4.6 x 10^{-3}	0.9 x 10^{-3}

* semi-quantitative ICP-MS measurements

Supplementary Table 6: Comparison of ICR of bare 316L and C-316L before and after being held at 0.9 V vs RHE in oxygen-saturated H_2SO_4 (pH 4.5) at 60 °C for 7 days.

	ICR* (as-received)	ICR* (after 7 days)
316L (1)	187 mΩ cm^2	926 mΩ cm^2
316L (2)	377 mΩ cm^2	1082 mΩ cm^2
C-316L (1)	2.1 ± 0.2 mΩ cm^2	2.3 ± 0.2 mΩ cm^2
C-316L (2)	2.1 ± 0.2 mΩ cm^2	1.9 ± 0.2 mΩ cm^2

* interfacial contact resistance vs. carbon-fibre GDL (1.4 MPa)

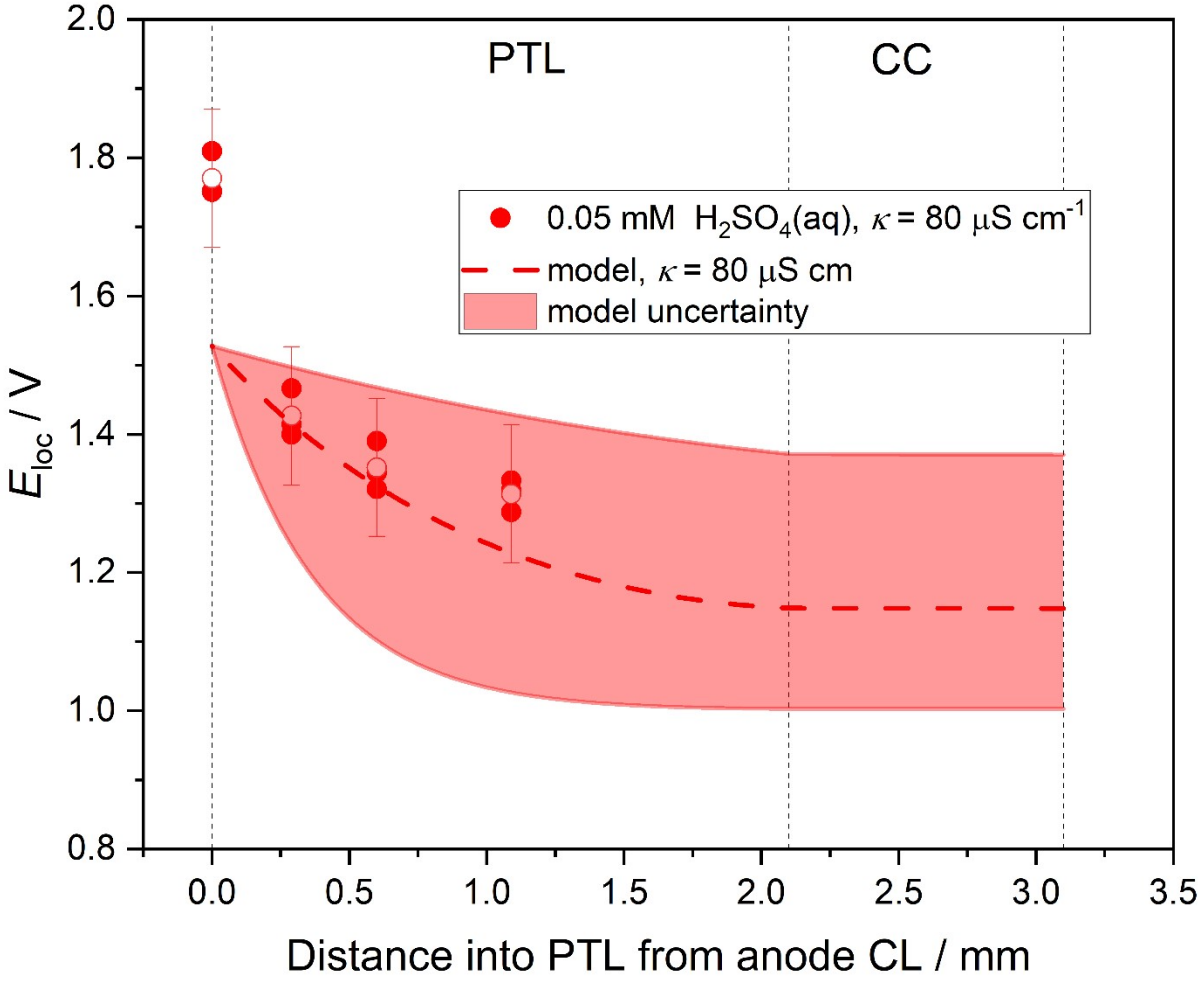

Supplementary Figure 1. Comparison of predicted (dashed line), measured (filled circles), and average of measured (open circles) local potential as a function of distance into the anode PTL in 0.05 mM H_2SO_4 at 60 °C. Error bars reflect the experimental measurement uncertainty, which is primarily associated with liquid junction potentials. The shaded area indicates the uncertainty in predicted E_{loc} due to PTL corrosion exchange current density and PTL volumetric surface area. The PTL is 2.1 mm thick and the mesh is 1 mm thick.

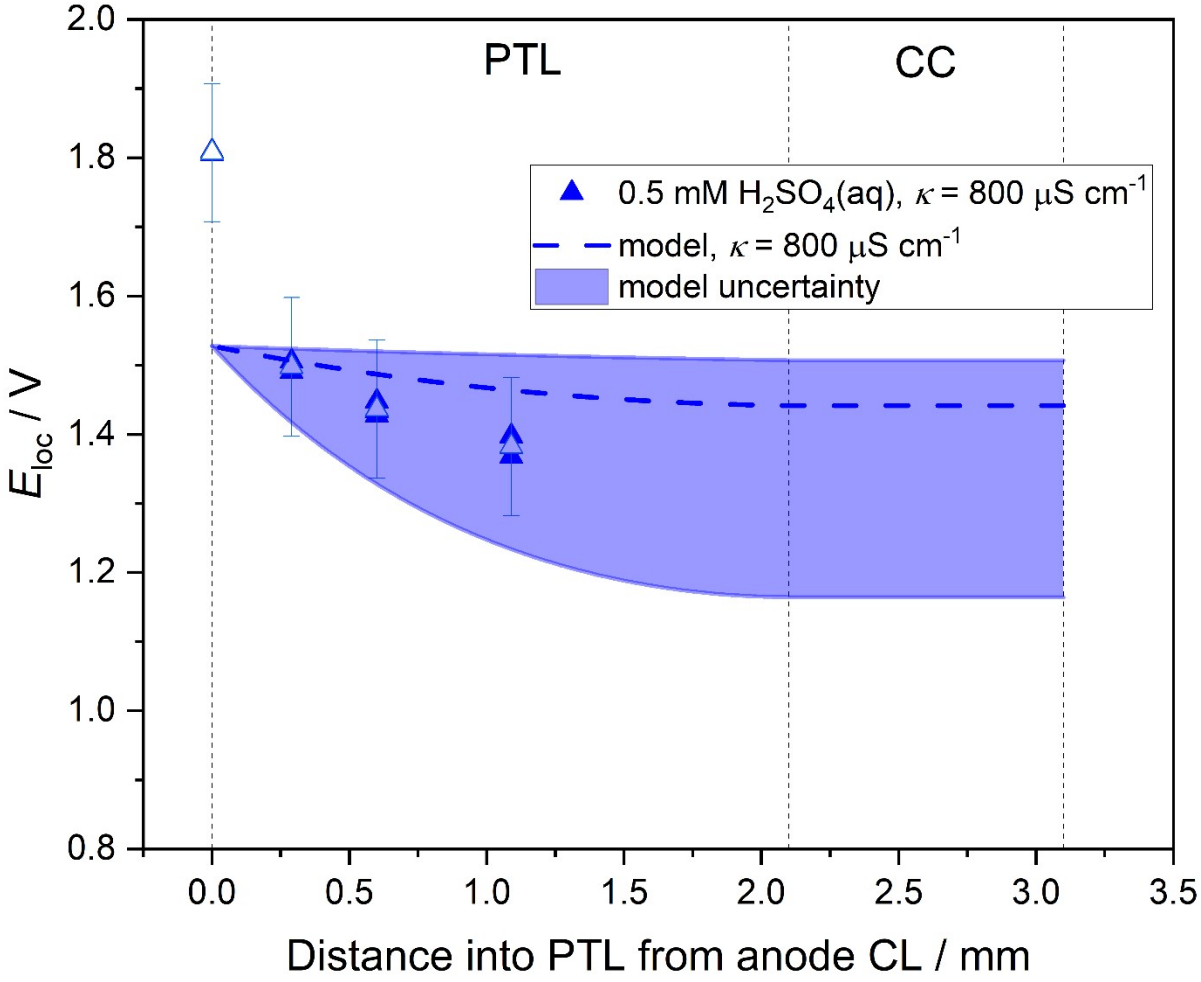

Supplementary Figure 2. Comparison of predicted (dashed line), measured (filled triangles), and average of measured (open triangles) local potential as a function of distance into the anode PTL in 0.5 mM H_2SO_4 at 60 °C. Error bars reflect the experimental measurement uncertainty, which is primarily associated with liquid junction potentials. The shaded area indicates the uncertainty in predicted E_{loc} due to PTL corrosion exchange current density and PTL volumetric surface area. The PTL is 2.1 mm thick and the mesh is 1 mm thick.

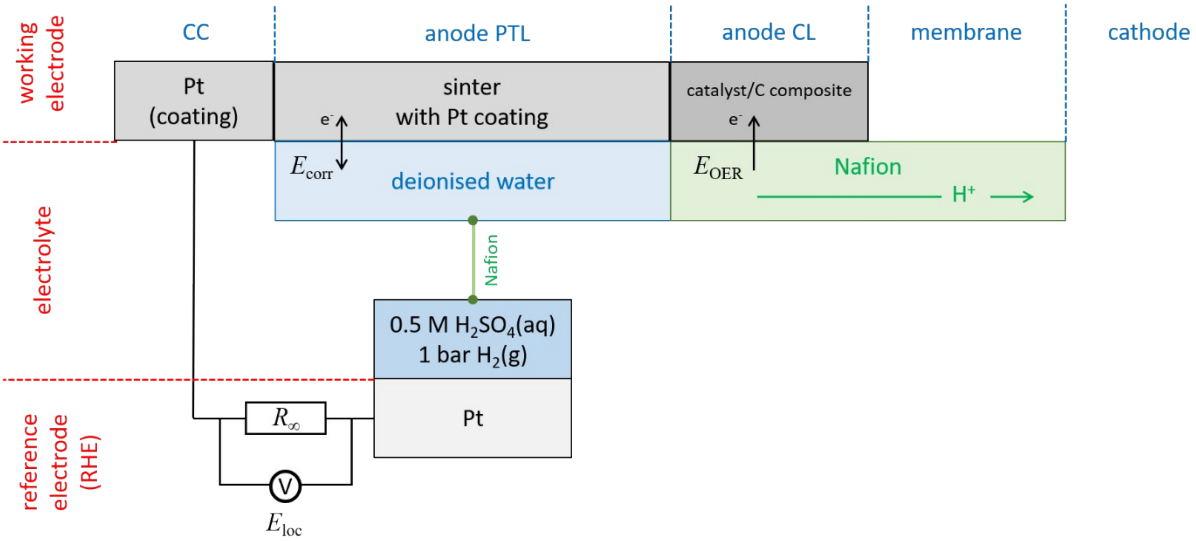

Supplementary Figure 3. Schematic illustration of conductive phases on the anode side of a PEMWE. The horizontal axis resolves different regions of the PEMWE device, while the vertical axis resolves different phases, which in porous media may have morphologically complex interfaces. Passive corrosion processes (oxidative material dissolution, oxide formation and oxygen reduction) are indicated by the potential E_{corr}; the oxygen evolution reaction is indicated by the potential E_{OER}.

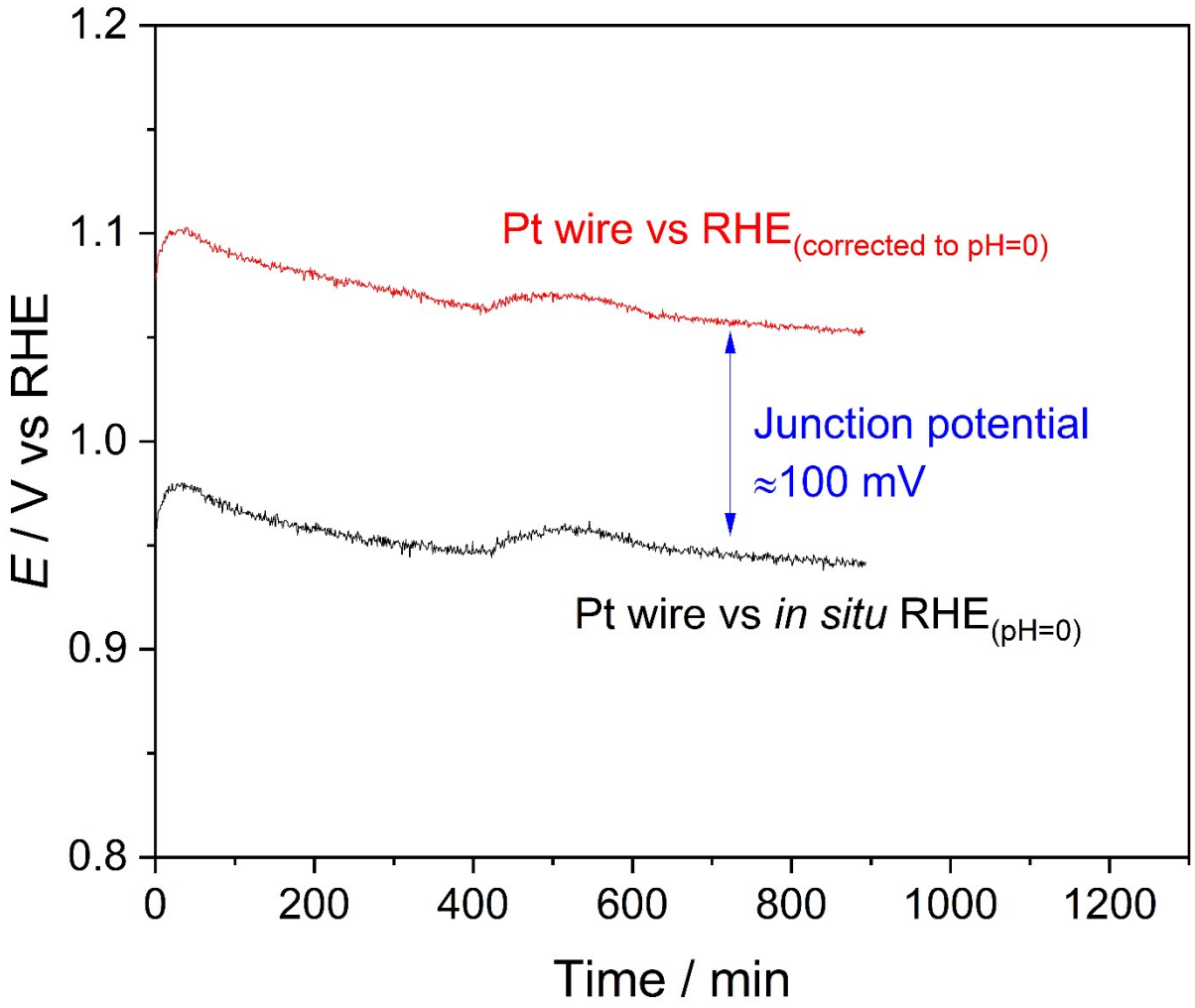

Supplementary Figure 4. *Ex situ* evaluation of magnitude of liquid junction potential. The OCP of Pt wire is measured against 2 reference electrodes: (i) RHE directly immersed in the electrolyte and (ii) RHE in 0.5 M H_2SO_4 connected with Nafion tubing into the electrolyte (as in the *in situ* reference electrode system used in the single cell tests). The electrolyte is 0.5 mM H_2SO_4 (measured pH of 2.7), 60 °C, oxygen-sparged.

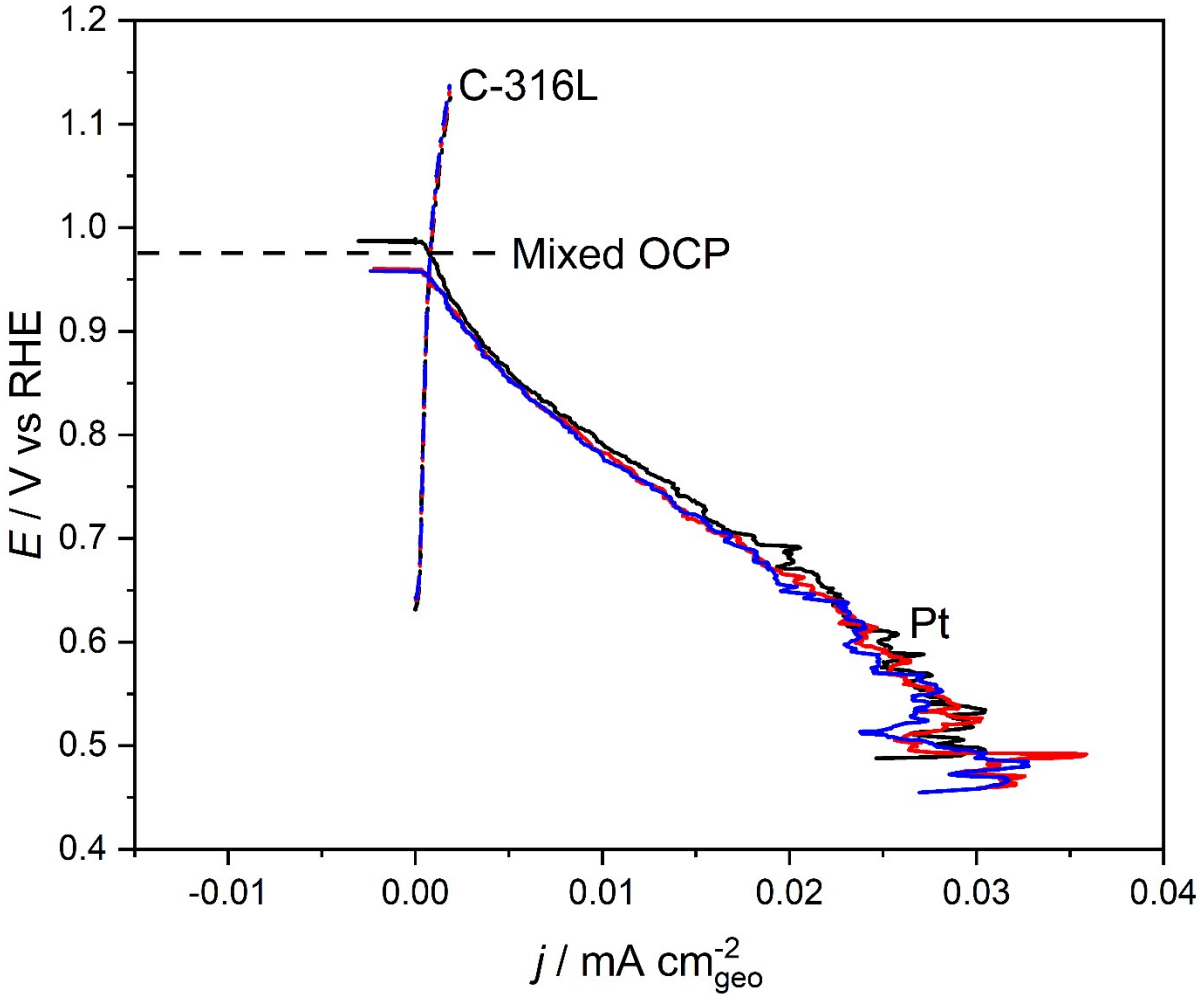

Supplementary Figure 5. Evans diagram of Pt-coated Ti PTL and C-316L; repeats are reported in different colours. All experiments were performed at pH = 4.5 (H_2SO_4), oxygen-sparged, 60 °C, with RHE connected using Nafion salt bridge. The faster kinetics of Pt/PtO formation pulls the mixed OCP closer to the OCP of Pt/PtO rather than that of C-316L.

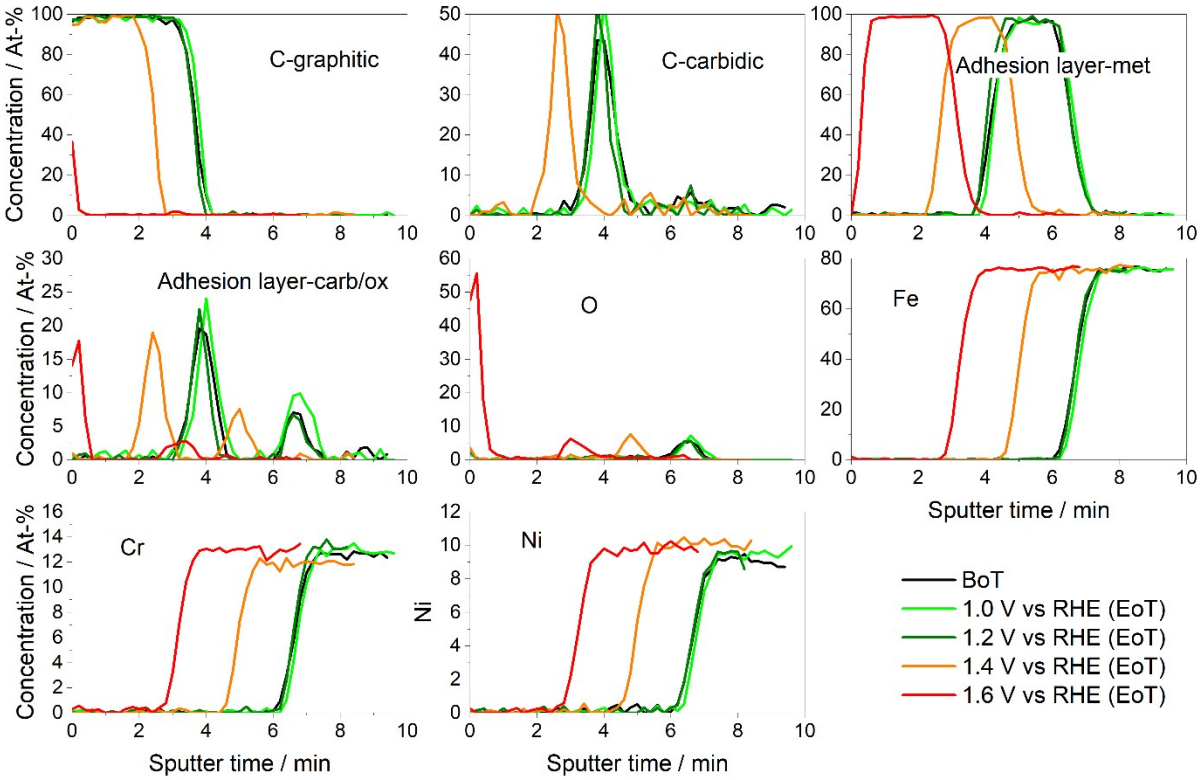

Supplementary Figure 6. AES sputter depth profiles of C-304L at beginning of the test (BoT, black) and end of the test (EoT) at 1.0 V vs RHE (green), 1.2 V vs. RHE (olive), 1.4 V vs RHE (orange), and 1.6 V vs RHE (red). The overlapping curves for carbon (graphitic and carbidic), adhesion layer (metallic, oxidic, and carbidic) and the substrate (Fe, Cr, and Ni) in the case of BoT and EoT at 1.0 V vs RHE and 1.2 V vs RHE demonstrate high stability of the coating at these potentials. In contrast, at 1.4 V vs RHE and 1.6 V vs RHE (orange and red curves) the carbon and other signals are shifted to lower sputtering times, indicating carbon removal.

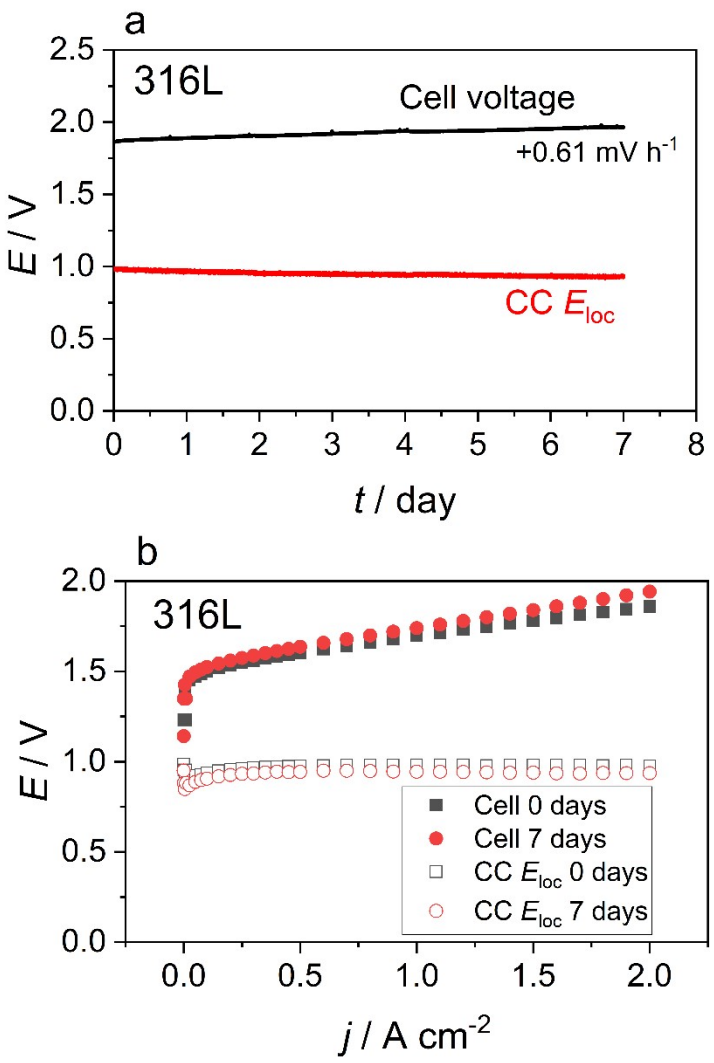

Supplementary Figure 7a. Evolution of cell voltage and E_{loc} in a single cell PEMWE with a bare 316L anode CC, operated at 2 A cm^{-2} for 7 days at 60 °C using Type I water allowed to equilibrate with air. **b.** Polarisation curves and E_{loc} measurements as a function of current density for the cell before and after the 7-day test. Both figures exhibit constant decoupling of E_{loc} and minimal cell degradation.

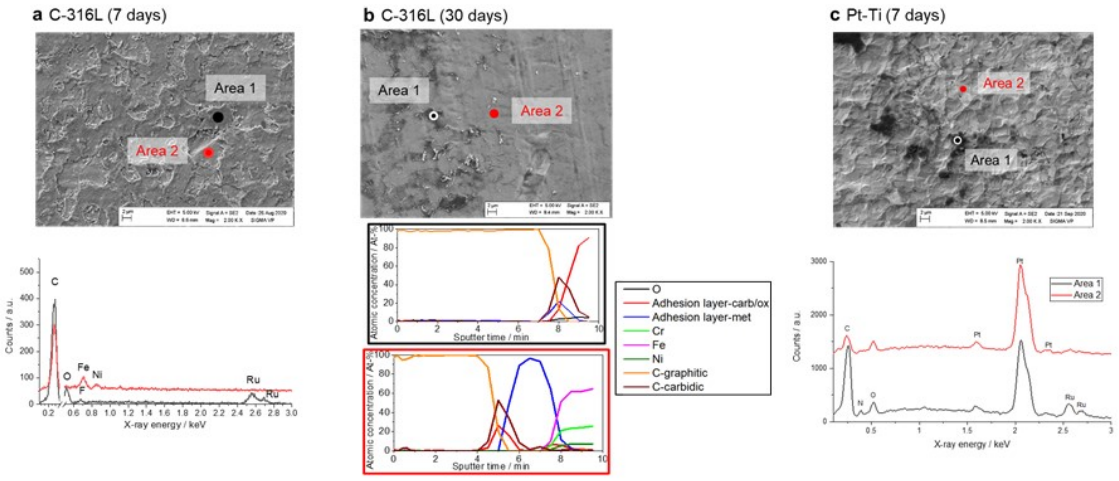

Supplementary Figure 8a. SEM image of the C-316L CC after the 7-day test, showing locations of two areas (black and red) for the corresponding EDS spot analysis shown. **b.** SEM image of the C-316L CC after the 30-day test, showing locations of two areas (black and red) for the AES sputter depth profiles shown. The latter exhibit a difference only in the carbon thickness, suggesting adventitious carbon contamination on top of the carbon coating. **c.** SEM image of the Pt-Ti CC after the 7-day test, showing locations of two areas (black and red) for the corresponding EDS spot analysis shown.

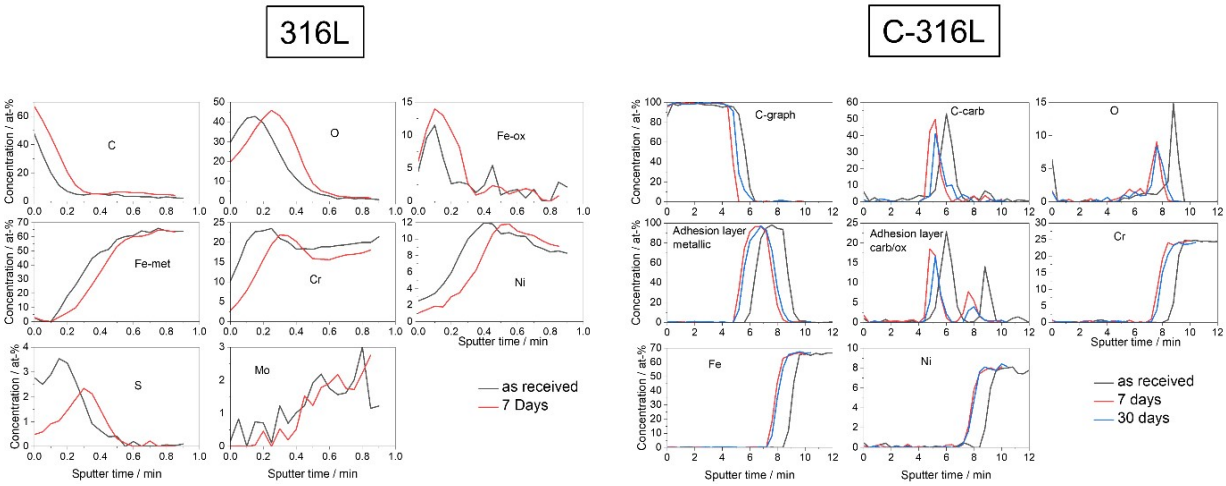

Supplementary Figure 9. Element by element comparison via AES depth profiles of bare 316L and C-316L anode CCs after single cell testing at 2 A cm^{-2}, 60 °C. **Left.** Comparison of AES depth profiles for the as-received 316L (black) and after the 7 day test (red). The slight shift of the elements to the right after 7 days is explained by the thicker carbon contamination of the sample, although the depth profile was acquired outside the heavily contaminated region. The stronger iron oxide (Fe-ox) signals suggest slight oxidation of the tested sample, but significant changes in surface composition are not detected. **Right.** Comparison of AES depth profiles for the as-received C-316L (black), after the 7 day test (red) and after the 30 day test (blue). The thickness of the graphitic carbon coating (C-graph) varies slightly in an unsystematic manner, which is attributed to different carbon thicknesses obtained from the coating process. This variation is within a few nanometres and, thus, bulk oxidation of carbon can be ruled out.

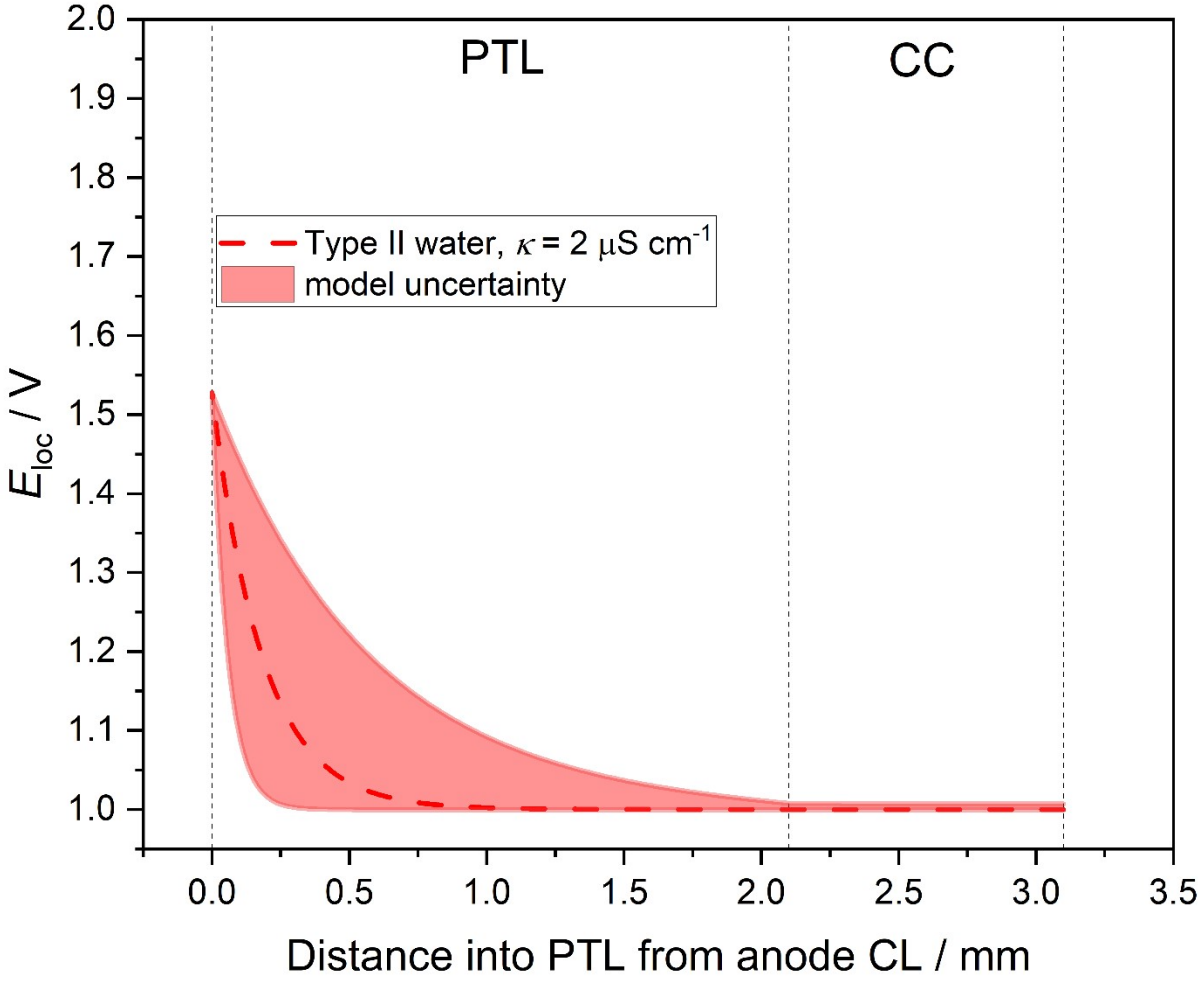

Supplementary Figure 10. Predicted potential profile (as measured between CC and an *in situ* RE, E_{loc}) through the anode PTL, for ASTM Type II water at 60 °C. Shaded area indicates the uncertainty in predicted E_{loc} due to PTL corrosion exchange current density and PTL volumetric surface area. The PTL is 2.1 mm thick and the mesh is 1 mm thick.

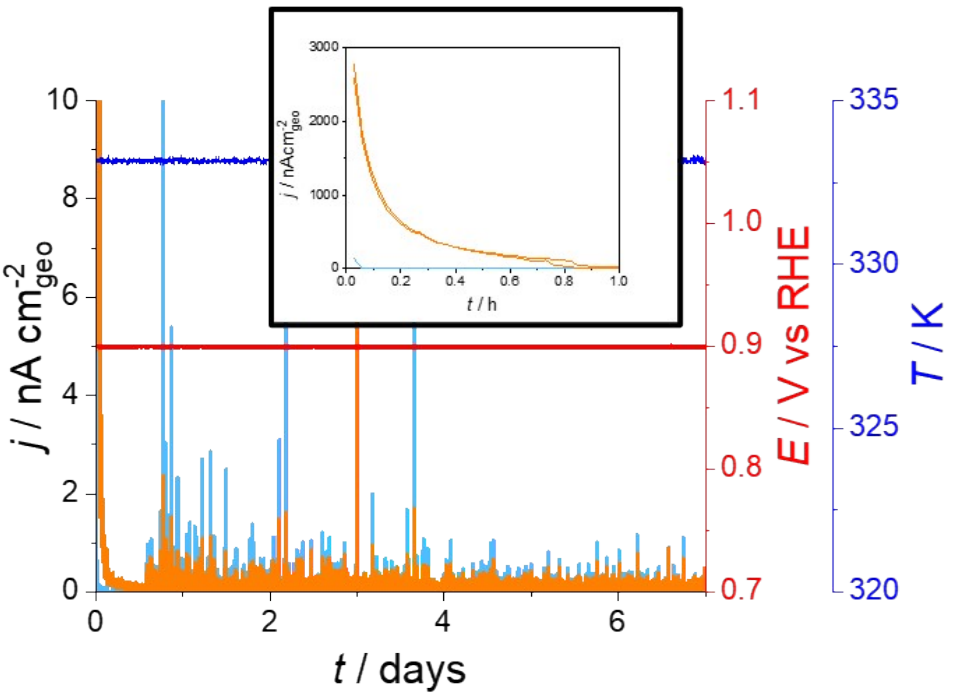

Supplementary Figure 11. Evolution of current density with time for bare 316L and C-316 at 0.9 V vs RHE, 60 °C, pH 4.5 (H_2SO_4), oxygen-saturated. Inset shows data from the first hour of the experiment.

Supplementary References

1 K. J. Vetter, *Electrochemical Kinetics: Theoretical and Experimental Aspects*, Academic Press Inc., New York / London, 1967.

2 H. Becker, L. Castanheira and G. Hinds, *J. Power Sources*, 2020, **448**, 227563.

3 A. Damjanovic, L. R. Yeh and J. F. Wolf, *J. Electrochem. Soc.*, 1982, **129**, 55–61.

4 ASTM Standard D 1125 - 95, *Standard Test Methods for Electrical Conductivity and Resistivity of Water*, 2005.